Journal of Renewable Energy and Environment

Research Article

Journal Homepage: www.jree.ir

Study of Long-Term Stability of Perovskite Solar Cells: Highly Stable Carbon-Based Versus Unstable Gold-Based PSCs

Mohammad Reza Shekari[a], Seyed Mohammad Sadeghzadeh[a], Mahdi Golriz[b*]

[a] *Department of Electrical Engineering, Shahed University, P. O. Box: 18155-159, Tehran, Tehran, Iran.*
[b] *Space Transportation Research Institute, Iranian Space Research Center, P. O. Box 13445-754, Tehran, Tehran, Iran.*

PAPER INFO

Paper history:
Received 03 Augustl 2020
Accepted in revised form 27 February 2021

Keywords:
Stability,
Efficiency,
Perovskite,
Electrode,
Carbon,
Solar Cell

ABSTRACT

In recent decade, Perovskite Solar Cells (PSCs) have received considerable attention compared to other photovoltaic technologies. Despite the improvement of Power Conversion Efficiency (PCE) of PSCs, the chemical instability problem is still a matter of challenge. In this study, we have fabricated two kinds of PSCs based on gold and carbon electrodes with the optimal PCE of about 15 % and 10.2 %, respectively. We prepared a novel carbon electrode using carbon black nanopowder and natural graphite flaky powder for Hole Transport Material (HTM) free carbon-based PSC (C-PSC). Current density-voltage characteristics over time were measured to compare the stability of devices. Scanning Electron Microscope (SEM) and Energy-dispersive X-ray Spectroscopy (EDS) analyses were carried out to study applied materials, layer, and surface structures of the cells. The crystal structure of perovskite and its association with the stability of PSCs were analyzed using an obtained X-ray diffraction (XRD) pattern. As a result, the constructed HTM-free C-PSC demonstrated high stability against air, retaining up to 90 % of its optimal efficiency after 2000 h in the dark under ambient conditions (relative humidity of (50 ± 5); average room temperature of 25 °C) in comparison to constructed gold-based PSCs (Gold-PSC) which are not stable at times. The experimental results show that novel low-cost and low-temperature carbon electrode could represent a wider prospect of reaching better stability for PSCs in the future.

https://doi.org/10.30501/jree.2021.240562.1132

1. INTRODUCTION

The general chemical formula for perovskite compounds is ABX_3, where A, B are two cations of very different sizes and X is an anion that bonds to both. For example, $CH_3NH_3PbI_3$ has very high light absorption capacity and offers proper electronic properties, which is a suitable candidate for Perovskite Solar Cells (PSCs). The structure has a band gap of 1.5 eV, which is proper for light absorption purposes [1]. The combination of the organic material + lead + halogen has attracted the attention of many researchers because of its special characteristics such as high absorption coefficient, the ability to adjust the band gap, high movement of the charges, and the distribution of electrons in nanostructured solar cells. The most common type of PSCs includes the FTO/compact TiO_2/mesoporous TiO_2/$CH_3NH_3PbI_3$/Hole Transporter Material (HTM)/back contact, as the back connection could be made by Au, Ag, carbon, etc. [2-8].

Study on PSCs was initiated by investigation of the Dye-Synthesized Solar Cells (DSSCs) in 2009 by A. Kojima et al., as the obtained efficiency of 3.8 % attracted the attention of the researchers and led to the extended studies in this field [9]. Higher efficiencies could be also obtained by substitution of the liquid electrolytes with the p-type solid spiro-MeOTAD [10-12]. Mixed halide perovskites including $CH_3NH_3PbI_{3-x}Cl_x$ and $CH_3NH_3PbI_{3-x}Br_x$ were also studied by the researchers and they resulted in the higher efficiency of PSCs because of greater electron-hole diffusion lengths in contrast to triiodide ($CH_3NH_3PbI_3$) perovskite absorber [13-15]. PSCs combined with other solar cell technologies such as tandem method could also achieve higher efficiency [16-17].

Although perovskite is promising, it has many disadvantages that limit its applications. The corrosion issues in contact with perovskite and silver, which results in the formation of silver halide, the high price of Au electrodes, and the need for the vacuum evaporation techniques, are some of the factors that limit the application of PSCs [18-20]. Also, the fabricating technology of this generation of cells still requires expensive metals such as Au and Ag as the electrodes, which are coated in vacuum conditions under thermal evaporation. Obviously, the high cost of these metals on a large scale and the need for enormous energy in the evaporation process in vacuum conditions will disrupt inexpensive techniques. Therefore, we would look for an appropriate alternative. The low-cost carbon would be an ideal material as a proper alternative to Au because of their similar performance. Graphite, carbon black, coal powder, carbon cloth, spongy carbon, and Carbon Nano-Tube (CNT) are well-known carbon materials that have been used as carbon electrodes in

*Corresponding Author's Email: m.golriz@isrc.ac.ir (M. Golriz)
URL: http://www.jree.ir/article_127112.html

Please cite this article as: Shekari, M.R., Sadeghzadeh, S.M. and Golriz, M., "Study of long-term stability of perovskite solar cells: Highly stable carbon-based versus unstable gold-based PSCs", ***Journal of Renewable Energy and Environment (JREE)***, Vol. 8, No. 2, (2021), 61-73. (https://doi.org/10.30501/jree.2021.240562.1132).

fabricating PSCs so far [21-24]. Accessibility, chemical stability, environmental friendliness, and controllable porosity are all advantageous features of carbon materials [25]. Low cost, high efficiency, and proper stability are the challenges of the researchers for development of the organic/inorganic PSCs [26]. Z. Li et al. laminated films of CNT network on $CH_3NH_3PbI_3$ substrate as a hole-collector using the vapor deposition chemical method. In the absence of an organic HTM and metal contact, they made a solar cell with an efficiency rate of up to 6.87 %. Meanwhile, preparation of the CNT electrode requires temperatures higher than 1150 °C [27]. The components including organic materials, lead, and halogens are unstable at high temperatures or in contact with some other solvents; hence, it is essential to apply a low-temperature method for the preparation of these materials [28]. Since perovskite is unstable at high temperatures or in contact with some solutions, preparation of the carbon layer will be challenging. The low-temperature electrode layer deposition on the perovskite could be used to select and optimize the material and structure of this type of cell without destroying its structure [29]. In 1996, for the first time, Gratzel and Kay reported a proper construction method of DSSCs in a continuous non-vacuum process by simple printing techniques using a carbon electrode and with an efficiency rate of 6.7 % [30]. In another report prepared by H. Zhou et al., the constructed cells represented optimal efficiency at about 9 % as their stability in the darkness was 2000 h. The possibility of constructing a carbon layer on a perovskite layer at lower temperatures (without damaging it) was also studied, thus facilitating the construction steps and increasing the possibility of stability [31]. As a result of the instability of the perovskite at temperatures higher than 150 °C, the carbon electrode could be deposited at low temperatures using doctor blade coating method [32]. Due to the bipolar characteristic of $CH_3NH_3PbI_3$, this material could act as a light absorber and hole transporter at the same time. Also, electron and hole are effectively injected into the n-type conductors and carbon electrode, respectively [33]. For the first time, L. Etgar et al. reported the preparation of HTM-free PSCs with an efficiency rate of 5 %, which proved that perovskite acted simultaneously as a light absorber and a HTM. The removal of HTM increases the stability and reduces costs as the manufacturing process becomes easier and the optimal efficiency for HTM-free cells reaches up to 10.85 % [34]. The conductivity and mechanical performance of the carbon layer play an important role in collecting the hole. Besides, in the case of using carbon derivatives in the carbon electrode layer and achieving an optimum thickness of carbon electrode, the series resistance of the cell with carbon electrode will decrease, which leads to an increase in efficiency [31, 35]. In 2013, Z. Ku et al. presented a report on the construction of a carbon electrode, which plays the role of a hole-conductor. They used carbon derivatives such as spheroidal and flaky graphite via a screen printing method. The results indicated that the solar cell with a carbon black/spheroidal graphite electrode was more stable and presented the efficiency of 6.64 %, which represented a better performance than the flaky graphite spheroidal-based device and made it comparable to a gold material version. Besides, filling up the pores of TiO_2 layers was done more efficiently by the spheroidal graphite than the flaky graphite. They also achieved proper stability in environmental conditions over 840 h [36]. They deposited the perovskite film using the dip-coating method and through diffusion into the carbon layer and ZrO_2 insulating layer. Then, they provided the conditions for drying the cell in a dark environment. They used the screen printing method for the other layers, including the carbon electrode layer, ZrO_2 and TiO_2 layers [37-38]. In this type of Carbon-based Perovskite Solar Cells (C-PSCs), since the thickness of the carbon layer affects the electrical conductivity, the researchers also tried to improve the Power Conversion Efficiency (PCE) of the cell by changing the thickness of the electrode layer [39]. Black carbon and graphite or a mixture of them (carbon paste) can be used a carbon electrode in the solar cells using film deposition methods such as the screen printing and doctor-blade coating. For example, in 2012, L. Zhang et al. studied the effect of particle size of graphite used in the carbon electrode on the efficiency of solar cells as well as the effect of electrode thickness and the PCE in optimum condition, which reached 11.65 % [40]. H. Wang et al. also studied the effect of carbon black and the dosage and percentage of carbon black and graphite in the electrode. They reached the highest efficiency (7.08 %) at 20 % of carbon black ratio, because carbon black would greatly influence the uniform formation of perovskite film. The efficiency remains relatively unchanged after 900 h, which indicates its proper stability [35].

The stability of PSCs is effectively related to the destruction of perovskite crystals over time. In general, given that perovskite is sensitive to moisture, the process of destruction is completed besides oxygen and light in the form of the following equations, where Eqs. 1 and 2 occur due to the moisture and Eq. 3 is caused by oxygen. Eq. 4 is accelerated under the effect of sunlight; therefore, all three factors increase the destruction trend besides each other. Changing the color of PSCs from black to light yellow over time represents the decomposition of perovskite crystals [41-45].

$$CH_3NH_3PbI_3\ (s) \leftrightarrow PbI_2\ (s) + CH_3NH_3I\ (aq) \quad (1)$$

$$CH_3NH_3I\ (aq) \leftrightarrow CH_3NH_2\ (aq) + HI\ (aq) \quad (2)$$

$$4HI\ (aq) + O_2\ (g) \leftrightarrow 2I_2\ (s) + 2H_2O\ (l) \quad (3)$$

$$2HI\ (aq) \leftrightarrow H_2\ (g) + I_2\ (s) \quad (4)$$

In 2019, X. Wu et al. improved the moisture stability and efficiency of the C-PSCs by inserting an inorganic Copper (I) thiocyanate (CuSCN) as an HTM between perovskite and carbon electrode to suppress the electron recombination process and using highly conductive CNT networks to form a robust interface of CuSCN/CNT and reached a PCE value up to 17.58 % [46]. Also, Q. Chu et al. developed an efficient low temperature, solution-processed Poly(3-hexylthiophene-2,5-diyl) P3HT/graphene Hole Transport Layer (HTL) for improving the hole transport and reported a record efficiency rate of 18.1 % for C-PSCs, which showed outstanding stability towards moisture, oxygen, and light [47]. Recently, S. Wang et al. reported that Cs^+ doping in methylammonium lead iodide perovskite ($Cs_xMA_{1-x}PbI_3$) led to the manufacturing of remarkably stable HTM-free C-PSC which maintained up to 90 % of its initial PCE under a high-humidity condition after 1000 h [48]. In terms of water polarity, destruction of perovskite crystals occurs even in a low-moisture environment and the deconstruction time is delayed; if not protected against moisture, they will rapidly decompose and the PCE of cell extremely decrease. Low-cost carbon electrode due to its hydrophobic nature prevents the diffusion of moisture into the structure of the cell and plays an

HTM role, which is cheaper than Au and spiro-MeOTAD. Carbon is almost purely based on aromatic and non-polar sheets such that the interaction of extremely polar molecules such as water is very weak and leads to hydrophobia of the carbon electrode surface and high contract angle with water drops [36, 49-50]. The contact angle of water on the carbon surface is 113°, which reflects its hydrophobicity. Also, the contact angle of water on the silver and gold surface is less than 90°, which shows that their hydrophilic surface is semi-wetted by water. Higher contact angles do not allow water to be distributed or absorbed on the surface; thus, it takes a drop shape and slides [31].

Apart from the thermal stability of perovskite, the thermal stability of the HTM matters and basically, inorganic protective and blocking layers are stable. In 2014, S.N. Habisreutinger et al. considered the resistance against water diffusion and thermal stability factors, attenuated thermal destruction, and improved the thermal stability by substitution of the organic HTM with the Single-Walled carbon Nano-Tubes (SWNTs), embedded in a polymer isolator, as the efficiency was improved by 15.3 % [51]. In 2016, A. Baranwal et al. fabricated a three-layer printable HTM-free PSC with a mesoporous carbon back contact and demonstrated the thermal stability over 1500 h at 100 °C using a side-sealing UV-curable encapsulation method [52]. Moreover, using $Cs_xFA_{1-x}PbBr_xI_{3-x}$ and $Cs_xNa_{1-x}PbI_3$ light absorber perovskites was reported by researchers to enhance the thermal stability of the HTM-free C-PSCs [53-54].

In this research, two types of PSCs based on the gold electrode (Gold-PSC with HTM) and carbon electrode (HTM-free C-PSC) were constructed. The objective of this work is to demonstrate the effect of carbon electrode on the stability of HTM-free C-PSC in comparison to the Gold-PSC with HTM as well as the variation of efficiency versus time in order to propose some solutions for improving stability. We applied a novel carbon paste containing carbon black nanopowder (Average Nanoparticle Size: 30 nm) and natural graphite flaky powder (approximately 3 µm) at a weight ratio of 2:3 and also obtained a thickness of 20 µm for carbon electrode using the doctor-blade coating method, which makes this study distinguishable from the other researches in terms of carbon electrodes.

2. EXPERIMENTAL

2.1. Meterials

In this work, the following materials were used: Titanium isopropoxide or TTIP ($Ti[OCH(CH_3)_2]_4$) with 97 % purity, density of 0.967 g/cm^3 (20 °C) from Sigma-Aldrich (Tetraisopropyl orthotitanate); Hydrochloric acid (HCl) with 37 % purity, density of 1.19 g/cm^3 (20 °C) from Merck; Ethanol (C_2H_5OH) with 99.9 % purity, density of 0.79 g/cm^3 (20 °C) from Merck (Ethyl alcohol); Lead (II) iodide (PbI_2) with 99.99 % purity, density of 6.16 g/cm^3 (25 °C) from Sigma-Aldrich (Plumbous iodide); Dimethylformamide or DMF ($HCON(CH_3)_2$) with 99.8 % purity, density of 0.94 g/cm^3 (20 °C) from Merck; Methylammonium iodide (CH_3NH_3I) with 99.9 % purity from Sigma-Aldrich; Isopropanol ($CH_3CH(OH)CH_3$) with 99.5 % purity, density of 0.786 g/cm^3 (20 °C) from Merck; Chlorobenzene (C_6H_5Cl) with 99 % purity, density of 1.105-1.107 g/cm^3 (d 20 °C/4 °C) from Sigma-Aldrich (Phenyl chloride); Spiro-OMeTAD ($N^2,N^2,N^{2'},N^{2'},N^7,N^7,N^{7'},N^{7'}$-octakis(4-methoxyphenyl)-9,9′-spirobi[9H-fluorene]-2,2′,7,7′-tetramine) with 99 % (HPLC) purity from Sigma-Aldrich; Bis(trifluoromethylsulfonyl)amine lithium salt (LiTFSl, $CF_3SO_2NLiSO_2CF_3$) with 99 % purity, density of 1.33 g/cm^3 from Sigma-Aldrich (Lithium bistrifluoromethanesulfonimidate); Acetonitrile (CH_3CN) with 99.8 % purity, density of 0.786 g/cm^3 from Sigma-Aldrich (Ethyl nitrile); 4-Tert-butylpyridine or TBP ($C_9H_{13}N$) with 98 % purity, density of 0.923 g/cm^3 (25 °C) from Sigma-Aldrich; Carbon black nanopowder (Average Nanoparticle Size: 30 nm) with 99 % purity from MTI Corporation; Natural graphite flaky powder (approximately 3 µm) with 99.9 % purity from US-Nano; Ethyl cellulose from Sigma-Aldrich; Terpineol ($C_{10}H_{18}O$) from Sigma-Aldrich; Zirconium oxide nanopowder (ZrO_2, APS: 20 nm) with 99.95 % purity, density of 5.89 g/cm^3 from US-Nano; Zinc powder (Zn) with 99.995 % purity from Sigma-Aldrich; Titanium tetrachloride or TTC ($TiCl_4$) with 99.9 % purity from Sigma-Aldrich; Transparent TiO_2 paste (20-25 nm particle size) from Sharif Solar; Fluorine doped tin oxide-coated glass slide (FTO glass) from Sigma-Aldrich; and acetone (CH_3COCH_3) with 99.8 % purity, density of 0.79 g/cm^3 (20 °C) from Merck (Dimethyl ketone).

2.2. Preparation procedures and deposition methods

Figures 1a and 1b represent two cross-sectional areas of a Gold-PSC with HTM and a HTM-free C-PSC, respectively. The main difference between the structures below is the use of an HTM (spiro-MeOTAD) in the Gold-PSC. The sequence of layers of the constructed cells is as follows:

a. Gold-PSC with HTM: FTO / Blocking Layer (compact TiO_2) / Mesoporous TiO_2 / Perovskite ($CH_3NH_3PbI_3$) / HTM (spiro-MeOTAD) / Au Electrode

b. HTM-free C-PSC: FTO / Blocking Layer (compact TiO_2) / Mesoporous TiO_2 / Perovskite ($CH_3NH_3PbI_3$) / Carbon Electrode

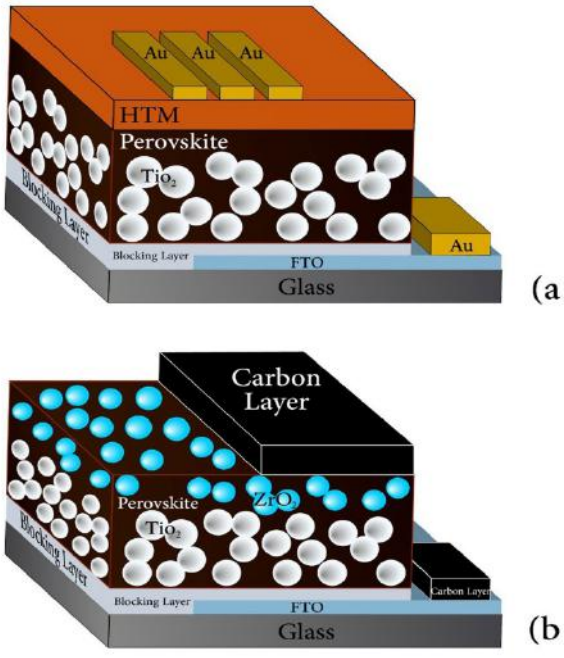

Figure 1. Cross-sectional structures of (a) the Gold-PSC with HTM and (b) the HTM-free C-PSC

First, we etched one side of the FTO glasses (each square part including 4 cells (1.4 cm × 1.4 cm)) by using HCl (2 M) and Zinc powder to prevent short circuits from occurring. Then, the etched glasses were washed in an ultrasonic bath. In this report, we have fabricated 6 PSCs including 5 Gold-PSCs with HTM and one HTM-free C-PSC. In order to prepare the mentioned structures, four types of solutions (block solution, lead iodide (PbI_2) solution, CH_3NH_3I solution, and spiro-MeOTAD solution) and one type of carbon ink were made and the thin films were deposited step by step. For the preparation of the block solution, we used TTIP, ethanol and, HCl. Also, the final block solution was filtered using a syringe filter (pore size: 220 nm). A proper dosage of the block solution was then poured on the FTO glass all at once and film deposition was blocked using a spin coater device starting at 2000 rpm for 30 s as the thickness of the layer reached about 40 nm. Afterward, one part of the cells parallel to the etched sides was cleaned by ethanol. In order to use the electrical connections, this part of the cells should be cleaned at the end of each film deposition process except perovskite film deposition. After heating the piece in the oven at 500 °C for 1 h, 4 cells were disconnected and the layers underwent treatment in the $TiCl_4$ solution for 30 min at 70 °C. For mesoporous TiO_2 film deposition, the TiO_2 paste diluted by ethanol at a weight ratio of 1:3.5 was deposited by spin coating method at 5000 rpm for 30 s. After that, the part of the cells which had been cleaned by ethanol in the previous film deposition was cleaned by ethanol again. Then, it was placed in the oven at 500 °C for half an hour. Once the temperature reached 70 °C, layers were removed and put on the hot plate; note that during the deposition of perovskite layers, the temperature should be fixed at 70 °C. Lead iodide solution including PbI_2 and DMF stirred at 70 °C for 12 h. It was then filtered using a syringe filter (pore size: 450 nm). We know that this solution should be kept at 70 °C during the film deposition process and if the temperature is lowered at this step, it becomes semi-crystalline immediately.

Perovskite film deposition was conducted by spin coating method using the PbI_2 solution at a speed of 6500 rpm for the duration of 5 s. The cells were then put in the oven at 70 °C for 30 min. After cooling down, the cells were placed inside the pre-prepared CH_3NH_3I solution at a concentration of about 10 mg/ml in isopropanol and the film deposition was conducted using dip-coating method. This way, each cell was placed inside the solution one by one for the duration of 20 s. Then, the cells were removed from the mentioned solution and placed inside the isopropanol solution. Finally, the devices were dried using the spin coater at a speed of 4000 rpm for 10 s and re-dried in the oven at 70 °C for 30 min.

For HTM film deposition of 5 Gold-PSCs, we prepared 2 solutions including spiro-MeOTAD in chlorobenzene and LiTFSI in Acetonitrile, respectively. After adding some TBP to the first solution, some of the second solution was also added to the obtained solution. Then, the last obtained spiro-MeOTAD solution was put under stirring at 60 °C for half an hour. Moreover, it was finally filtered using a syringe filter (pore size: 220 nm). Spiro-MeOTAD film deposition was conducted by spin coating method at 4000 rpm for the duration of 30 s. At this step, the cleaned part of the cells was gently cleaned again using the acetone solution. After passing 12 h from the deposition of spiro-MeOTAD, Au electrode film deposition for the 5 Gold-PSCs was conducted using the vacuum evaporation method.

For electrode film deposition of the HTM-free C-PSC after the perovskite film deposition, prepared carbon ink was deposited by a doctor-blade method, in which a sticker (with 30 µm thickness size) was also applied for reaching a thickness of 20 µm.

2.3. Preparation of carbon ink

For the preparation of the carbon paste, 2 g of carbon black nanopowder mixed with 3 g of natural graphite flaky powder and 0.5 g of ethyl cellulose was added to 25 g of Terpineol. Initially, to evaporate the solvents that exist in carbon paste, it was put in the oven for 12 h at 120 °C to prevent any possible reaction of perovskite with the solutions existing in carbon paste; this is because Terpineol material used in the carbon paste could destroy the perovskite immediately. In order to prepare carbon ink, 5 g of pre-dried carbon paste was mixed with 4 g of ZrO_2 nanopowder and 15 ml of chlorobenzene, which was then milled for 2 h to be completely homogenized.

2.4. Measurement and analysis devices

2.4.1. Current density-voltage (J-V) characterization

We used an IV-curve tracer from IRASOL to obtain current density-voltage (J-V) curves where solar simulator from IRASOL and power meter were used. We provided the following parameters for the cells using these devices: short-circuit current density (J_{SC}), open-circuit voltage (V_{OC}), the voltage at which the maximum power occurs (V_{max}), the current density at which the maximum power occurs (J_{max}), maximum power (P_{max}), efficiency of solar cell (PCE or η %), Fill Factor (FF) or the ratio of maximum obtainable power to the product of the open-circuit voltage and short-circuit current, and series resistance due to electrodes' connection (R_S). Eq. 5 and Eq. 6 show separately calculations of PCE and FF [16].

$$\text{PCE}\ (\eta\ \%) = \frac{J_{max}\cdot V_{max}}{P_{in}} * 100 = \frac{J_{sc}\cdot V_{oc}\cdot FF}{P_{in}} * 100 \quad (5)$$

$$FF = \frac{J_{max}\cdot V_{max}}{J_{sc}\cdot V_{oc}} \quad (6)$$

The manufactured cells have been tested under standard experimental conditions (T=25 °C and under AM1.5 conditions; intensity of incident light (P_{in})=100 $mW.cm^{-2}$). Both during the test and at the time of keeping the cells in a dark condition for stability analysis, the relative humidity in the laboratory is (50 ± 5) %.

2.4.2. SEM and EDS characterization

Samples were coated with Au and their morphologies were studied using Scanning Electron Microscope (SEM) images. Moreover, Energy-dispersive X-ray Spectroscopy (EDS) analyses were obtained using a Field-Emission Scanning Electron Microscope (FE-SEM) from TESCAN (MIRA3).

2.4.3. X-ray diffraction (XRD)

X-Ray Diffraction (XRD) pattern was obtained using an X-ray diffractometer from GNR (Explorer). Films were scanned in the reflection mode using an incident X-ray of Cu Kα (40 KV and 30 mA) with a wavelength of 1.54 A° at a step size of 0.01° and a scan rate of 1°/min from 2θ = 5° to 100°.

3. RESULTS AND DISCUSSION

Figures 2a and 2b indicate the 5 Gold-PSCs (No. 1-5) and the HTM-free C-PSC (No. 6) constructed in this research, respectively. During the construction of the cells, we have studied different thicknesses and layer surfaces in various film depositing conditions to obtain the optimum layer in terms of thickness, quality, and uniformity. The blocking layer was the first layer studied for construction which is necessary for preventing recombination of electrons and the generated holes due to radiation and it also controls electron loss in contrast to the FTO and the perovskite layer. If this layer is very thinner (less than 25 nm), it cannot quickly release photoelectrons, which leads to a decrease in J_{SC} and, thus, a reduction in PCE. Moreover, if this layer is highly thick (more than 80 nm), it leads to increased resistance in the path of photoelectrons. Thus, the photovoltaic performance of the cells extremely depends on the thickness of this layer [55-56].

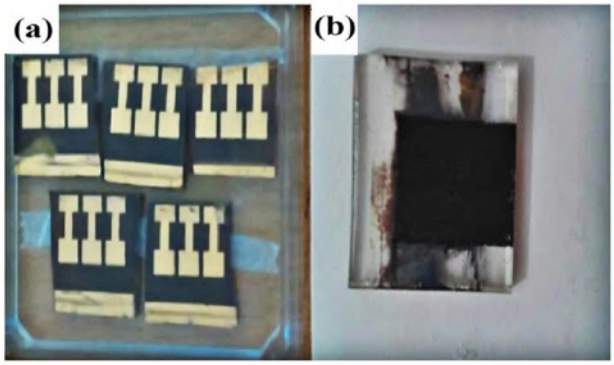

Figure 2. Constructed cells including (a) the 5 Gold-PSCs (No. 1-5) and (b) the HTM-free C-PSC (No. 6)

According to the studies of other researchers, we know that the optimal photovoltaic parameter occurs when the thickness of block layer is between 40 and 80 nm [57]. We achieved a thickness in this range using experimental experiences as follows. First, we tested 2.5 ml and 2 ml of block solution for 2 FTO glasses and the thickness of the prepared blocking layer for each FTO glass was obtained as about 140 nm and 100 nm, respectively. Therefore, these cases were not proper for construction purposes. SEM images of the surface and the thickness of the blocking layer for each case are observed in Figures 3 a-d. Then, blocking layer deposition was taken using 1 ml of the block solution for a new case as the thickness of the layer reached a little more than 40 nm. Figures 4a and 4b indicate the surface and the cross-section images of the blocking layer in this condition, where the thickness seems adequate for PCE goals.

The mesoporousTiO_2 layer or the second film deposited in this research is effective in formation of the perovskite structure. In this report, the thickness of this layer was obtained about 250 nm, which is proper for the construction of the PSCs. This layer could also be deposited using alternative materials like Al_2O_3. M. Lee et al. reported using Al_2O_3 instead of mesoporous TiO_2 and obtained similar efficiency in 2012 [58]. The surface and the cross-section SEM images of the mesoporous TiO_2 layer are separately shown in Figures 4c and 4d. The TiO_2 films (mesoporous TiO_2 layer + blocking layer) range is specified in Figure 4d, where the total thickness is about 300 nm. TiO_2 mesoporous film thickness could be changed by variation in TiO_2 paste concentration by adding ethanol. Depletion region for the PSCs is a region some part of which is inside the mesoporous TiO_2 layer and another part is inside the perovskite layer and consists of n and p areas. If we consider the thickness of mesoporous TiO_2 film less than 250 nm, in so far as perovskite penetrates inside mesoporous TiO_2 layer, the thickness of the depletion region severely decreases, which leads to severe efficiency reduction [59-60]. The thickness of the mesoporous TiO_2 layer affects the thickness of the perovskite layer because perovskite diffuses into this structure and perovskite crystals will form there. Some parts of perovskite also are formed on this layer and a total thickness of 300 nm is obtained. The thickness of the perovskite layer on mesoporous TiO_2 layer is about 350 nm. According to the morphology of the TiO_2 films (Figs. 4a and 4c), it is illustrated that TiO_2 nanoparticles size is smaller in mesoprous film than block film. Therefore, the specific surface area of the mesoprous film is higher than that of blocking film.

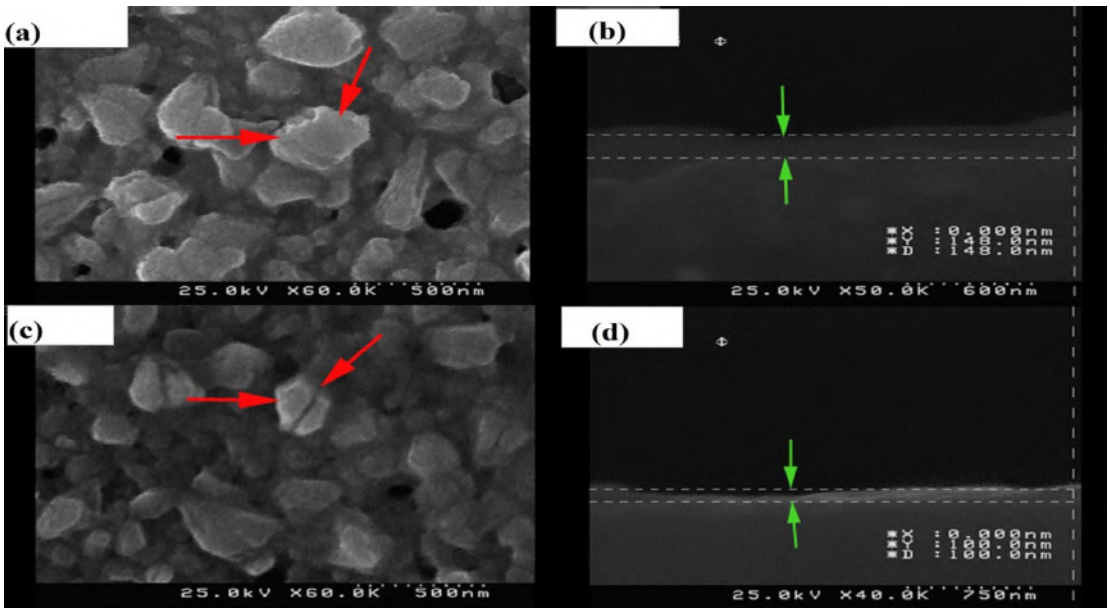

Figure 3. (a) The surface and (b) the cross-section SEM images of the blocking layer for deposition of 2.5 ml of the block solution, (c) the surface, and (d) the cross-section SEM images of the blocking layer for deposition of 2 ml of the block solution

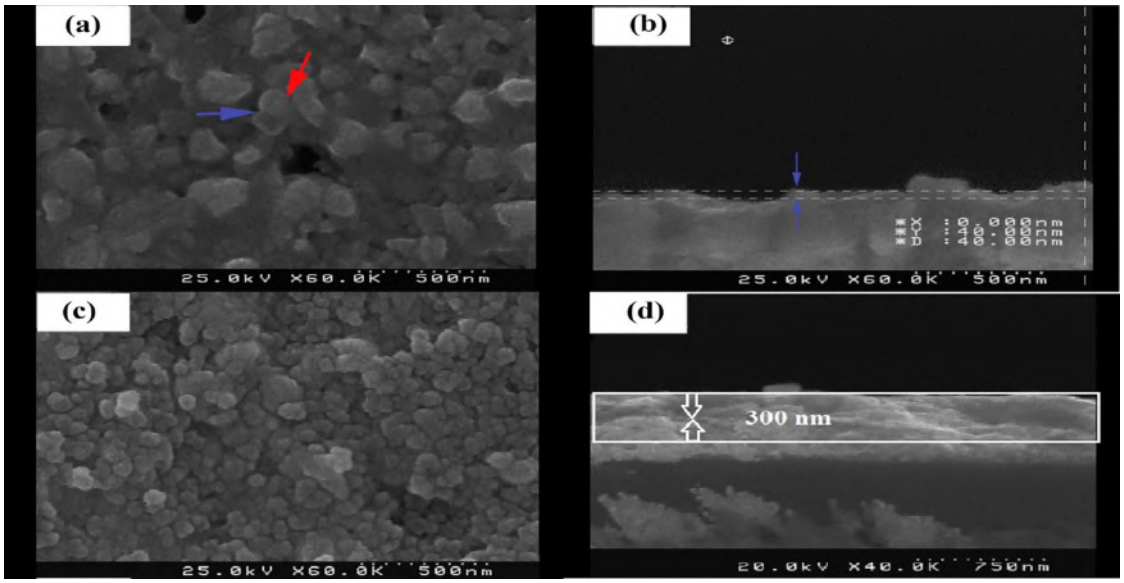

Figure 4. (a) The surface and (b) the cross-section SEM images of the blocking layer for deposition of 1 ml of the block solution; (c) the surface and (d) the cross-section SEM images of the mesoporous TiO_2 layer

In order to better understand the PSCs structure, one of the Gold-PSCs (cell No. 4) was tested through cross-section and surface analyses using an FE-SEM, and the results of EDS analysis are presented below. This cell was also broken for a cross-sectional image and its cross-section was covered with gold using Desk Sputter Coater. Figure 5a is an image of cell No. 4 broken from the cross-section. The variation in cell color results from decomposition of perovskite and its conversion to PbI_2 crystals. The cell surface on a scale of 2 mm is seen with specified areas of A and B in Figure 5b, in which area B is located on the Au electrode and area A is placed on the other surface of the cell. Besides, the area A where area C is specified and the area B are separately shown in Figures 5c and 5d on a scale of 5 µm. The results of EDS analysis for areas C and B could be seen in Figures 5e and 5f, respectively. Regarding the penetration depth defined for the FE-SEM during EDS analysis, the existing elements from the top layer to the down layer are specified in both analyses and the difference between two analyses is the gold in area B.

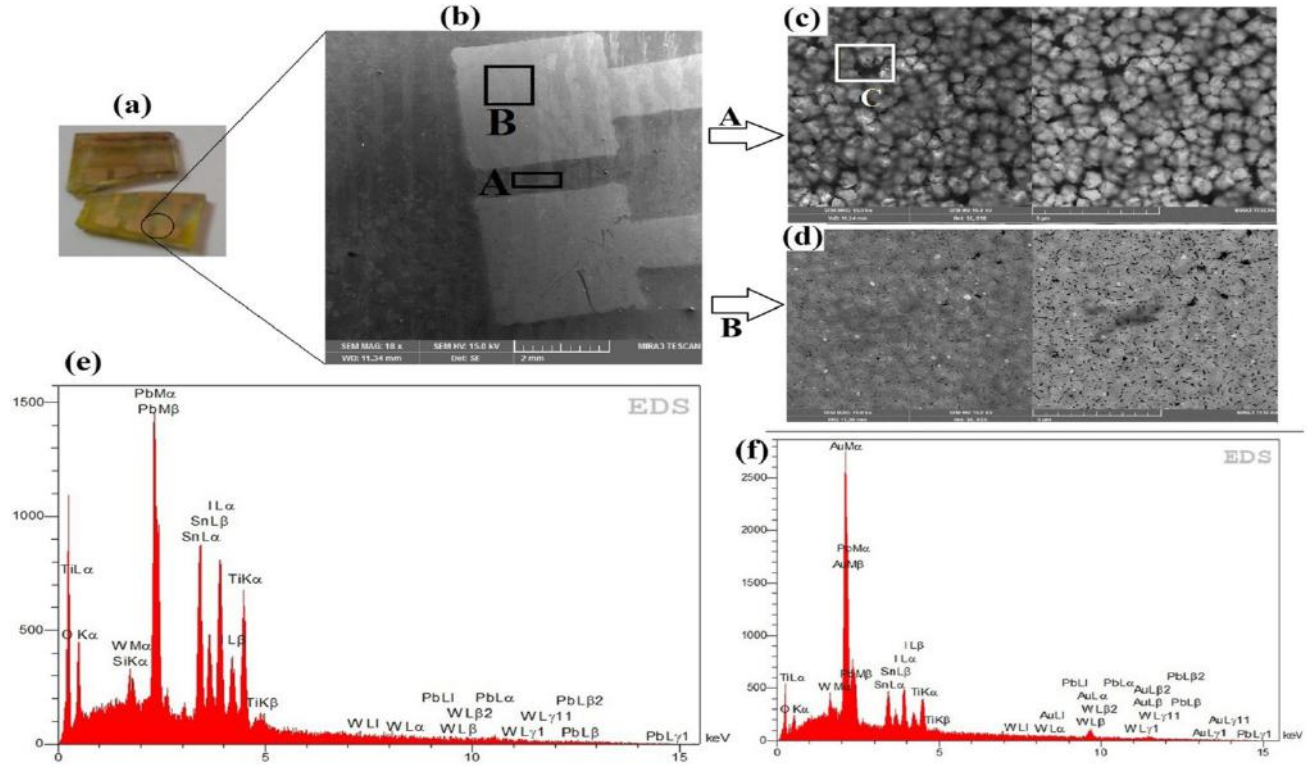

Figure 5. Images of (a) the broken cell No. 4 and (b) its surface on a scale of 2 mm; Top-view SEM images of the areas (c) A and (d) B on a scale of 5 µm; EDS analyses of the areas (e) C and (f) B

In Figure 6a, a cross-sectional image of cell No. 4 on a scale of 1 µm is seen where type of each layer and its thickness are specified and PbI_2 crystals could be seen in the place of perovskite. EDS analysis related to area D specified in the cross-sectional image is shown in Figure 6b. W, Al, and Sn are elements of FTO glass that are specified by the apparatus

(FE-SEM/EDS system) and the rests are the elements related to cell construction.

Five Gold-PSCs (No. 1-5) were tested three times after construction immediately and their photovoltaic parameters are shown in Table 1.

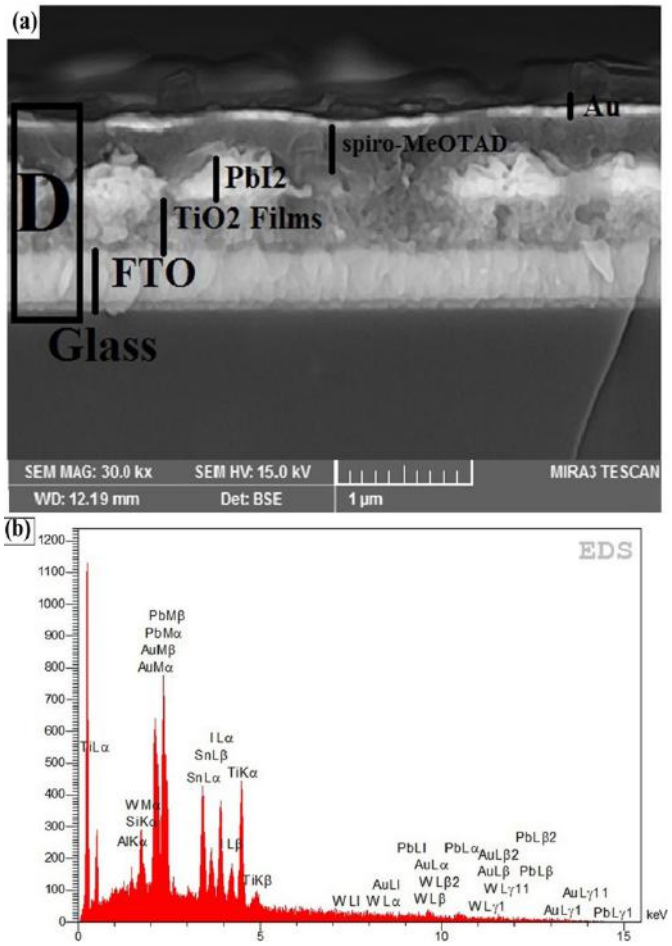

Figure 6. (a) The cross-sectional SEM image of the cell No. 4 and (b) EDS analysis of the area D

Table 1. Photovoltaic parameters of the 5 Gold-PSCs (No. 1-5) after construction

Cell number	V_{OC} (V)	J_{SC} (mA/cm^{-2})	FF	PCE (%)
1	0.96	20.4	0.69	13.51
	1.02	21.68	0.62	13.74
	0.98	21.88	0.59	12.58
2	1.08	23.25	0.54	13.6
	1.04	21.93	0.49	11.31
	1.13	23	0.55	14.32
3	1.03	24.12	0.57	14.25
	1.05	**24.2**	**0.59**	**14.95**
	1.04	24.52	0.58	14.88
4	0.99	20.42	0.67	13.56
	1.02	20.58	0.66	14.01
	1.01	19.74	0.67	13.42
5	1.15	18.1	0.68	14.31
	1.15	19.48	0.65	14.59
	1.12	17.68	0.6	11.95
Average	1.05	21.4	0.61	13.66
Standard deviation	**± 0.06**	**± 2.16**	**± 0.06**	**± 1.03**

The average PCE for these cellswas 13.66 % and cell No. 3 enjoyed optimal efficiency which was about 15 % at V_{OC} of 1.05 V, J_{SC} of 24.2 mA.cm^{-2}, and FF of about 0.59. The photovoltaic parameters of the HTM-free C-PSC (cell No. 6) were also measured after construction including V_{OC} = 0.89 (V), J_{SC} = 17.88 (mA.cm^{-2}), FF = 0.53, and PCE = 8.56 %. Figures 7a and 7b show the current density-voltage (J-V) graphs of the optimum Gold-PSC (cell No. 3) and cell No. 6 after construction under both illumination and dark conditions.

Figure 8 indicates an SEM image of the cross-sectional area of cell No. 6, in which the 20 µm thickness of the carbon layer is obvious. Cell No. 6 could be compared with similar research by H. Zhou et al. in which a 20.6 µm thickness average of carbon electrode led to optimal efficiency for HTM-free C-PSC [31]; however, they only used commercial conductive carbon paste for preparing carbon ink and achieved an average PCE of about 7 %.

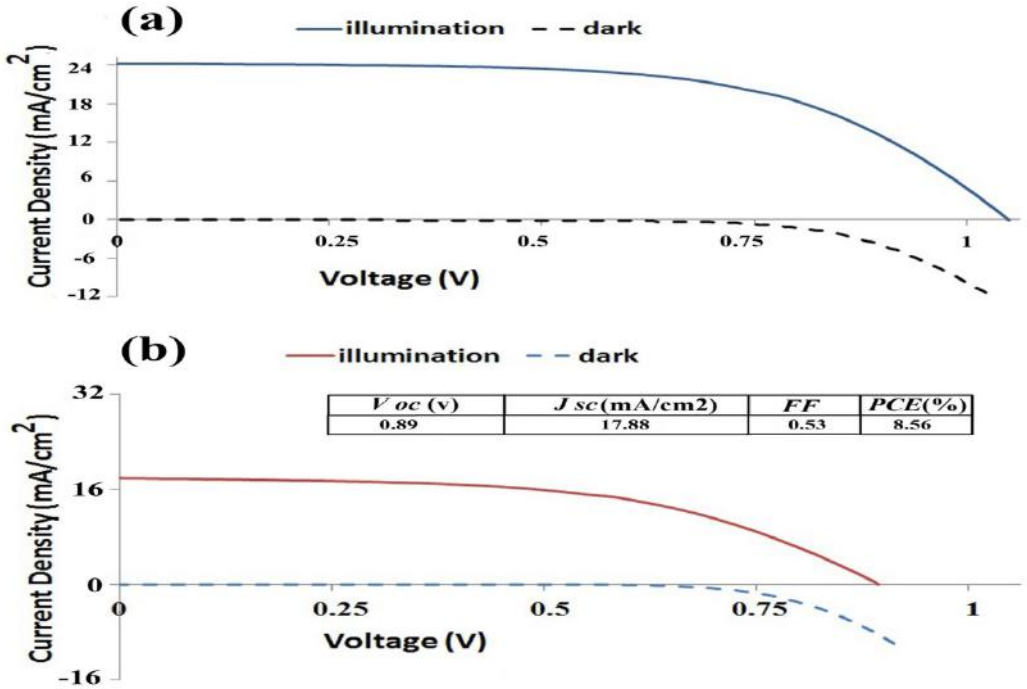

Figure 7. J-V graphs of (a) cell No. 3 and (b) cell No. 6 after construction under both illumination and dark conditions

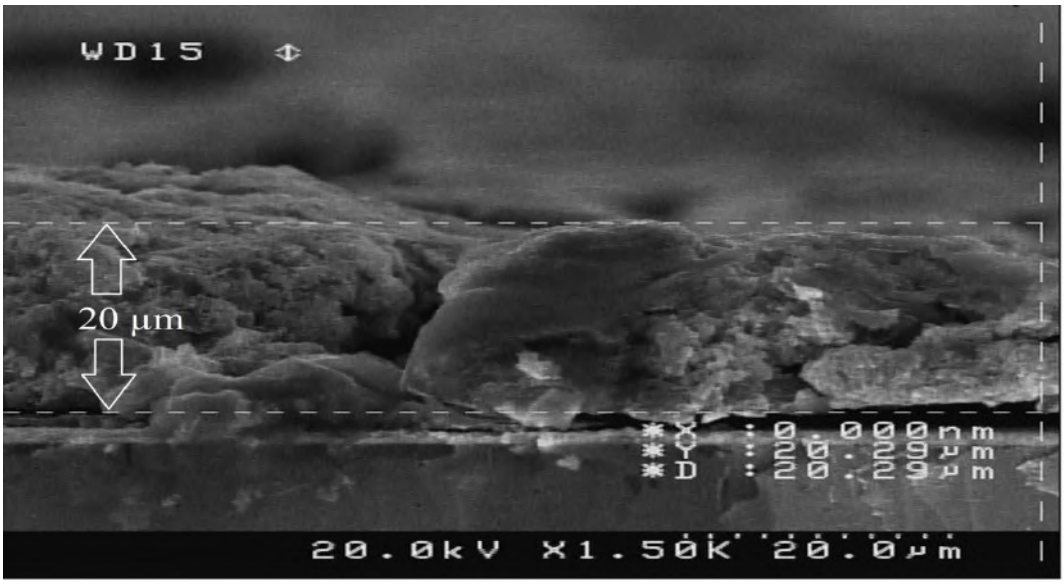

Figure 8. The cross-sectional SEM image of cell No. 6

The series resistance of solar cells could be calculated from their data and J-V graphs. R_S values of cell No. 3 and cell No. 6 under illumination conditions are calculated:

$R_{s_{cell\ No.3}} = 79\ \Omega$, $R_{s_{cell\ No.6}} = 105\ \Omega$

The higher series resistance for cell No. 6 is one reason for its lower efficiency since high series resistance leads to a decrease in J_{SC} and thus, a reduction in efficiency.

Table 2 shows the properties of cells No. 6 and No. 3 kept in a dark condition after construction at time intervals. The table itself indicates that the cell with carbon electrode experiences lower variations of the photovoltaic parameters than the cell with Au electrode; therefore, cell No. 6 is more stable. Furthermore, the parameters of cell No. 6 increased during 48 h after construction, which reflects the positive effect of the carbon layer on the performance of PSC. The PCE of cell No. 6 experienced a maximum value of 10.2 % after 48 h. Table 2 indicates that the photovoltaic parameters of cell No. 6 were slightly reduced after 2000 h. On the contrary, parameters of cell No. 3 including J_{SC}, V_{OC}, and FF were reduced when compared to the initial data. According to Eq. 5, by reducing the photovoltaic parameters, the efficiency also decreased. Since the reduction of PCE over time is significant, cell No. 3 has not adequate stability.

After deposition of carbon ink (pre-dried carbon paste + ZrO_2 nanopowder + chlorobenzene) on the perovskite layer, the newly deposited carbon electrode starts to penetrate into the perovskite film until to be completely dried;thus, we could obtain better electrical conductivity and optimum efficiency after 48 h. The positive effect of carbon electrode implies reaching better conductivity after 2 days and it is an advantage that is not observed for gold electrode.

Table 2. Variation of the parameters of cell No. 3 and cell No. 6 over the time

Cell No. 3				**Cell No. 6**			
PCE (%)	V_{OC} (V)	J_{SC} (mA/cm^{-2})	FF	PCE (%)	V_{OC} (V)	J_{SC} (mA/cm^{-2})	FF
14.95	**1.05**	**24.2**	**0.59**	8.56	0.89	17.88	0.53
12.33	1.01	20.56	0.58	9.52	0.91	18.1	0.57
10	0.98	20.31	0.49	**10.2**	**0.94**	**18.4**	**0.59**
6.1	0.97	19.56	0.31	9.69	0.93	18.36	0.56
5.01	0.91	17.47	0.31	9.66	0.93	18.34	0.56
3.22	0.88	14.78	0.24	9.36	0.92	18.3	0.55
2.43	0.66	9.48	0.38	9.24	0.92	18.26	0.55
1.14	0.58	7.68	0.25	9.2	0.9	18.01	0.56

Cell No. 6 with carbon electrode deposited by a doctor-blade method including 40 % of carbon black nanopowder (30 nm) and 60 % of natural flaky graphite powder (3 µm) showed a proper PCE in comparison to the same devices for other researchers who applied various mixtures of carbon black and graphite in terms of percentage and particle size as the carbon electrode with different thicknesses for fabricating HTM-free C-PSCs [32, 35, 36, 40, 61-65]. Z. Liu et al. [32], H. Wang et al. [35], Z. Ku et al. [36], G. Yue et al. [61], Z. Liu et al. [62], X. Chang et al. [63], and J. Li et al. [64] manufactured various HTM-free C-PSCs with optimized PCEs of 6.88 %, 7.08 %, 6.64 %, 7.29 %, 6.21 %, 5 %, and 10.4 %, respectively. H. Wang et al. [35] obtained their optimum C-PSC using drop-coated perovskite and a printed carbon electrode with a thickness of 5 µm made of 20 % of carbon black and 80 % of flaky graphite powder. Z. Liu et al. [32] prepared the optimum carbon film mixed with graphite flakes (10 µm), nano-graphite powder (40 nm) and carbon black powder (40 nm) at a weight ratio of 1:2:1, which was printed with a thickness of 65 µm; in another research [62], they improved the initial PCE of their carbon/graphite-based device from 6.21 % to 8.61 % by packaging with polydimethylsiloxane (PDMS). The HTM-free C-PSC made by G. Yue et al. [61] indicated that the mass fraction of 25 % carbon black particles on the surface and interspace of graphite flakes could improve the charge transfer by creating the most suitable contact sites with the perovskite layer and thus, could increase PCE of the device up to 7.29 %.

Figure 9 represents the variation of PCE and FF overtime for cell No. 3 and cell No. 6. J-V graphs of cell No. 6 at different time intervals are seen in Figure 10a, reflecting high stability as well. In addition, graphs of the variation of J_{SC} and V_{OC} are also shown at the inset. Cell No. 6 achieved a PCE value of 9.2 % which maintained 90 % of its optimal performance after 2000 h. J-V graphs of cell No. 3, which is not stable, show significant variations in Figure 10b and PCE is considerably reduced from 15 % to 1.14 % after 2000 h. Therefore, the above results represent that cell No. 6 is more stable and low-cost than the Gold-PSCs in this research and is comparable with some other newly constructed HTM-free C-PSCs during the last two years in terms of stability [24, 44, 48, 54, 66-70]. For example, the optimized device made by X. Wu et al. [46] retained over 80 % of its initial performance under a relative humidity of (80 ± 10) % after 1000 h of continuous illumination of one sun condition or the low-cost coal-based device manufactured by F. Meng et al. [24] maintained over 80 % of its initial PCE and achieved a PCE value of 8.60 % after 120 h in an ambient atmosphere at room temperature (humidity 30 %). Other recent HTM-free C-PSCs fabricated by J. Liu et al. [67], B. Zong et al. [68], and X. Zhang et al. [69] retained 85 % (after 55 days under dark conditions (23 °C and 30 % humidity)), 96 % (after 576 h in an atmosphere with humidity of about 45 %), and 95 % (after 20 days in air (relative humidity of 25 %-35 %)) of their initial efficiency, respectively.

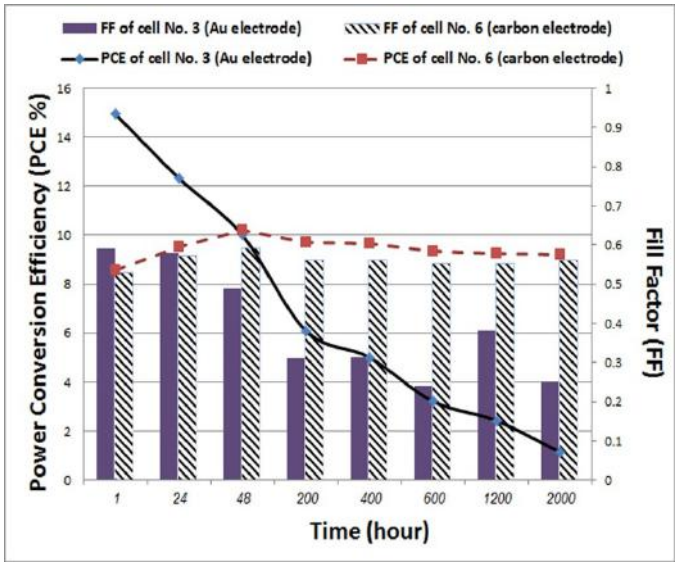

Figure 9. Variation of PCE and FF versus time for cell No. 3 and cell No. 6

In order to better understand the concept of stability and the sensitivity of the stability of PSCs, cell No. 5 was taken out of keeping place after 3000 h. This point should be mentioned that the keeping place of the cells is in a dark place under relative humidity of (50 ± 5) % at the average temperature of 25 °C which is suitable condition for controlling the stability of cells. Then, the decision was made on performing XRD analysis for cell No. 5. The original XRD pattern for cell No. 5 is seen in Figure 11a. Furthermore, Figure 11b shows an XRD pattern (Log-Scale for vertical axis) in which peaks are labeled by name and Miller indices (hkl). Here, for the XRD pattern, there are 27 peaks out of which 15 cases are related to TiO_2 and PbI_2. All peaks related to TiO_2, PbI_2, and Au are specified in the graph and it is obvious that SnO_2 and SiO_2 peaks are related to FTO glass.

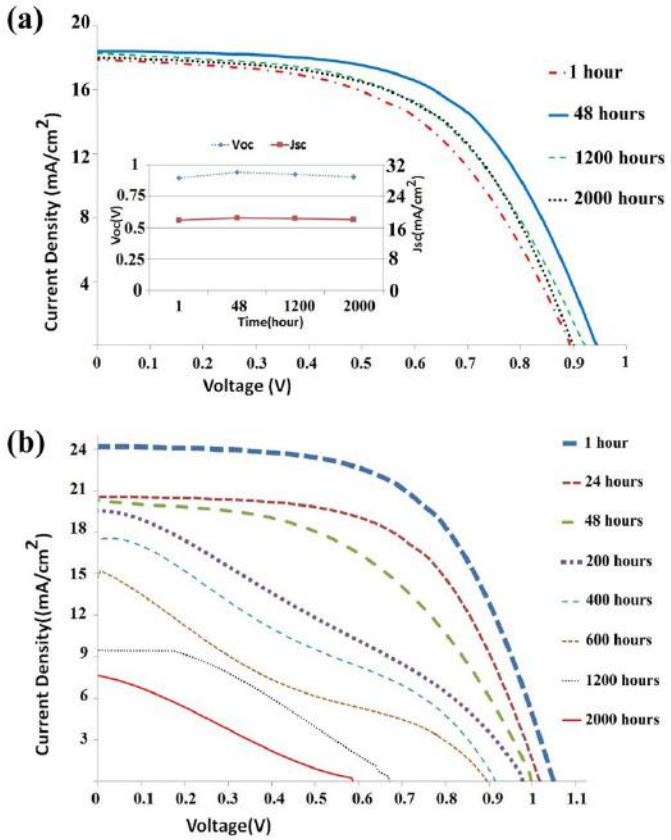

Figure 10. J-V graphs of (a) cell No. 6 and (b) cell No. 3 over time

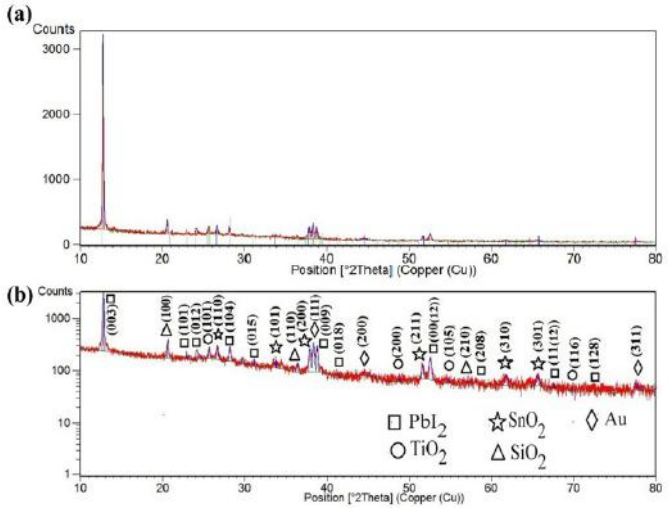

Figure 11. (a) Original XRD pattern for cell No. 5 and (b) with Log-Scale for vertical axis on which peaks are labeled by name and Miller indices (hkl)

Values of 2θ related to the peaks of each layer are presented in Table 3a in which the peaks specified with * are the highest peaks for each layer. Table 3b shows values of 2θ, θ, COS(θ), β or FWHM (°), β or FWHM (radian) related to the highest peaks for TiO_2 (JCPDS card no. 21-1272. The reason for the presence of mixed phase of TiO_2 is that we used amorphous TTIP for the preparation of the block solution and PbI_2 (JCPDS card no. 07-0235) is specified. FWHM is the integral breadth of a reflection (in radians 2θ) located at 2θ; this quantity is also sometimes denoted by Δ (2θ).

Here, by using XRD pattern (X'Pert HighScore Plus software) and by interpretation of Debye-Scherrer method, average crystallite size for TiO_2 and PbI_2 is calculated. As is

known, the average crystallite size is calculated by Debye-Scherrer equation in the form of Eq. 7 [71-75], where D is the average crystallite size in Ångström (Å), λ is the X-ray wavelength in Ångström (Å), β or FWHM is the peak width of the diffraction peak profile at half maximum height resulting from small crystallite size in radians and K is a constant related to crystallite shape, normally taken as 0.9. The value of β on 2θ axis of diffraction profile must be in radian. This can be attributed to the fact that "crystallite size" is not synonymous with "particle size", while X-Ray diffraction is sensitive to the crystallite size inside the particles. Since anode material of X-ray diffractometer is copper (Cu), λ value is 1.54 (Å). (λ = 1.54 (Å) = 0.154 nm).

$$D = \frac{K.\lambda}{\beta.\cos(\theta)} \quad (7)$$

$$D_{TiO_2} = \frac{0.9*1.54\ (Å)}{0.97511*0.00247} = 576\ (Å) = 58\ nm$$

$$D_{PbI_2} = \frac{0.9*1.54\ (Å)}{0.99379*0.00075} = 1859\ (Å) = 186\ nm$$

According to the Debye-Scherrer equation, the average crystallite size for TiO_2 and PbI_2 crystals is about 58 nm and 186 nm, respectively. As observed, the results exhibited that perovskite crystals of cell No. 5 were completely decomposed and were replaced by PbI_2 crystals with the average crystallite size of 186 nm after 3000 h, which demonstrated unstable properties of the Gold-PSCs.

Table 3. Values of (a) 2θ related to the peaks of each layer and (b) 2θ, θ, COS(θ), β or FWHM (°) , β or FWHM (radian) related to the highest peaks of TiO_2 and PbI_2

(a)	**2θ (°) related to the peaks**					
PbI_2	**12.7690***	22.8672	24.1230	28.1308	31.0825	38.7830
	41.4030	52.5087	58.5630	67.5930	72.8330	
TiO_2	**25.6203***	48.7630	54.6830	69.7930		
SnO_2	26.6404	33.7440	**37.8630***	51.5712	61.8423	65.6005
SiO_2	**20.5946***	36.3864	57.0430			
Au	**38.3079***	44.6031	77.6930			
(b)	**2θ (°)**	**θ (°)**	**COS (θ)**	**FWHM (°)**	**FWHM (radian)**	
PbI_2	12.7690	6.3845	0.99379	0.04309	**0.00075**	
TiO_2	25.6203	12.8101	0.97511	0.14191	**0.00247**	

4. CONCLUSIONS

In summary, we have successfully manufactured two types of PSCs including five Gold-PSCs based on Au electrode and one HTM-free C-PSC based on carbon electrode. The five Gold-PSCs showed an average initial PCE of 13.66 % and the optimum Gold-PSC achieved high PCE of about 15 %, whereas the HTM-free C-PSC exhibited an initial PCE value of 8.56 %, which is less than that of Gold-PSCs because of its higher series resistance (R_S), leading to a decrease in J_{SC} and the reduction of PCE. For fabricating the HTM-free C-PSC, a kind of carbon paste consisting of carbon black nanopowder (30 nm) and natural flaky graphite powder (3 μm) was developed at a weight ratio of 2:3 and it was applied to deposition of carbon electrode by a doctor-blade method with a thickness of 20 μm. The PCE value of the HTM-free C-PSC experienced a moderate rise up to 10.2 % within 48 h followed by a gradual drop to 9.2 % after 2000 h which demonstrated outstanding stability over the period in the dark under ambient conditions (relative humidity of (50 ± 5) %, average room temperature of 25 °C) because of retaining up to 90 % of its optimal PCE. In the same period, the PCE value of the optimized Gold-PSC declined dramatically to 1.14 %, which proved unstable behavior over time toward air and moisture. This study indicated complete destruction of perovskite crystals and conversion to PbI_2 crystals using XRD analysis. More importantly, the constructed HTM-free C-PSC was comparable with other newly constructed devices in terms of stability. The present work paves the way for developing low-cost and highly-stable PSCs in the future and is also helpful to improve the efficiency of C-PSCs further.

5. ACKNOWLEDGEMENT

This article was extracted from the Master's thesis prepared by Mohammadreza Shekari. The authors gratefully acknowledge the financial support for this work that was provided by Shahed University and Non-metallic Material Research Department of Niroo Research Institute. The authors would like to thank Iranian Space Research Center (ISRC) for their support and contribution to this study. We thank the Analytical and Testing Center of Sharif Solar (IRASOL) for J-V measurements. Also, the authors thank Razi Applied Science Foundation for FE-SEM images, EDS analyses, and XRD pattern.

REFERENCES

1. Almora, O., Vaillant-Roca, L. and Garcia-Belmonte, G., "Perovskite solar cells: A brief introduction and some remarks", ***Revista Cubana de Fisica***, Vol. 34, No. 1, (2017), 58-68. (http://revistacubanadefisica.org/index.php/rcf/article/view/RCF_34-1_58).
2. Chouk, R., Haouanoh, D., Aguir, C., Bergaoui, M., Toubane, M., Bensouici, F., Tala-Ighil, R., Erto, A. and Khalfaoui, M., "Dye sensitized TiO_2 and ZnO charge transport layers for efficient planar perovskite solar cells: Experimental and DFT insights", ***Journal of Electronic Materials***, Vol. 49, No. 2, (2020), 1396-1403. (https://doi.org/10.1007/s11664-019-07839-7).
3. Wei, H. and Huang, J., "Halide lead perovskites for ionizing radiation detection", ***Nature Communications***, Vol. 10, No. 1066, (2019). (https://doi.org/10.1038/s41467-019-08981-w).
4. Kang, A.K., Zandi, M.H. and Gorji, N.E., "Fabrication and degradation analysis of perovskite solar cells with graphene reduced oxide as hole transporting layer", ***Journal of Electronic Materials***, Vol. 49, (2020), 2289-2295. (https://doi.org/10.1007/s11664-019-07893-1).
5. Maleki, E, Ranjbar, M. and Kahani, S.A., "The effect of antisolvent dropping delay time on the morphology and structure of the perovskite layer in the hole transport material free perovskite solar cells", ***Progress in Color, Colorants and Coatings***, Vol. 14, No. 1, (2021), 47-54. (https://dx.doi.org/10.30509/pccc.2021.81671).
6. Sarvari, R., Agbolaghi, S. and Massoumi, B., "Engineered organic halide perovskite solar cells by incorporation of surface‐manipulated graphenic nanosheets", ***Journal of Materials Science: Materials in Electronics***, Vol. 30, No. 10, (2019), 9281-9288. (https://doi.org/10.1007/s10854-019-01258-4).

7. Sarvari, R., Agbolaghi. S. and Massoumi, B., "Role of graphene ordered modifiers in regulating the organic halide perovskite devices", ***Optical Materials***, Vol. 92, (2019), 81-86. (https://doi.org/10.1016/j.optmat.2019.04.014).
8. Agbolaghi, S., "Efficacy beyond 17 % via engineering the length and quality of grafts in organic halide perovskite/CNT photovoltaics", ***New Journal of Chemistry***, Vol. 26, No. 43, (2019), 10567-10574. (https://doi.org/10.1039/C9NJ02074H).
9. Kojima, A., Teshima, K., Shirai, Y. and Miyasaka, T., "Organometal halide perovskites as visible-light sensitizers for photovoltaic cells", ***Journal of the American Chemical Society***, Vol. 131, No. 17, (2009), 6050-6051. (https://doi.org/10.1021/ja809598r).
10. Corpus-Mendoza, A.N., Cruz-Silva, B.S., Ramirez-Zúñiga, G., Moreno-Romero, P. M., Liu, F. and Hu, H., "Use of magnetic fields for surface modification of PbI_2 layers to increase the performance of hybrid perovskite solar cells", ***Journal of Electronic Materials***, Vol. 49, (2020), 3106-3113. (https://doi.org/10.1007/s11664-020-08009-w).
11. Ankireddy, K., Lavery, B.W. and Druffel, T., "Atmospheric processing of perovskite solar cells using intense pulsed light sintering", ***Journal of Electronic Materials***, Vol. 47, (2018), 1285-1292. (https://doi.org/10.1007/s11664-017-5893-y).
12. Heo, J.H., Im, S.H., Noh, J.H., Mandal, T.N., Lim, C.S., Chang, J.A., Lee, Y.H., Kim, H.J., Sarkar, A., Nazeeruddin, Md.K., Grätzel, M. and Seok, S.-Il, "Efficient inorganic–organic hybrid heterojunction solar cells containing perovskite compound and polymeric hole conductors", ***Nature Photonics***, Vol. 7, No. 6, (2013), 486-491. (https://doi.org/10.1038/nphoton.2013.80).
13. Thakur, N., Mehra, R. and Devi, C., "Efficient design of perovskite solar cell using parametric grading of mixed halide perovskite and copper iodide", ***Journal of Electronic Materials***", Vol. 47, (2018), 6935-6942. (https://doi.org/10.1007/s11664-018-6620-z).
14. limi, B., Mollar, M., Marí, B. and Chtourou, R., "Thin film of perovskite (mixed-cation of lead bromide $FA_{1-x}MA_xPbBr$) obtained by one-step method", ***Journal of Electronic Materials***", Vol. 48, (2019), 8014-8023. (https://doi.org/10.1007/s11664-019-07638-0).
15. Phan Vu, T., Nguyen, M.T., Nguyen, T.T., Vu, T.D., Nguyen, D.L., An, N.M., Nguyen, M.H., Sai, C.D., Bui, V.D., Hoang, C.H., Truong, T.T., Lai, N.D. and Tran, T.N., "Three-photon absorption induced photoluminescence in organo-lead mixed halide perovskites", ***Journal of Electronic Materials***", Vol. 46, (2017), 3622-3626. (https://doi.org/10.1007/s11664-017-5407-y).
16. Hadadian, M., Smått, J.H. and Correa-Baena, J.P., "The role of carbon-based materials in enhancing the stability of perovskite solar cells", ***Energy & Environmental Science***, Vol. 13, No. 5, (2020), 1377-1407. (https://doi.org/10.1039/C9EE04030G).
17. Hosseinnezhad, M., "Enhanced performance of dye-sensitized solar cells using perovskite/DSSCs tandem design", ***Journal of Electronic Materials***, Vol. 48, (2019), 5403-5408. (https://doi.org/10.1007/s11664-019-07272-w).
18. Leijtens, T., Eperon, G.E., Pathak, S., Abate, A., Lee, M.M. and Snaith, H.J., "Overcoming ultraviolet light instability of sensitized TiO_2 with meso-superstructured organometal tri-halide perovskite solar cells", ***Nature Communications***, Vol. 4, No. 1, (2013), 1-8. (https://doi.org/10.1038/ncomms3885).
19. Domanski, K., Correa-Baena, J.P., Mine, N., Nazeeruddin, Md.K., Abate, A., Saliba, M., Tress, W., Hagfelft, A. and Grätzel, M., "Not all that glitters is gold: Metal-migration-induced degradation in perovskite solar cells", ***ACS Nano***, Vol. 10, No. 6, (2016), 6306-6314. (https://doi.org/10.1021/acsnano.6b02613).
20. Lee, J., Singh, S., Kim, S. and Baik, S., "Graphene interfacial diffusion barrier between CuSCN and Au layers for stable perovskite solar cells", ***Carbon***, Vol. 157, (2020), 731-740. (https://doi.org/10.1016/j.carbon.2019.10.101).
21. Cao, K., Zuo, Z., Cui, J., Shen, Y., Moehl, T., Zakeeruddin, S.M., Grätzel, M. and Wang, M., "Efficient screen printed perovskite solar cells based on mesoscopic $TiO_2/Al_2O_3/NiO$/carbon architecture", ***Nano Energy***, Vol. 17, (2015), 171-179. (https://doi.org/10.1016/j.nanoen.2015.08.009).
22. Zhang, N., Guo, Y., Yin, X., He, M. and Zou, X., "Spongy carbon film deposited on a separated substrate as counter electrode for perovskite-based solar cell", ***Materials Letters***, Vol. 182, (2016), 248-252. (https://doi.org/10.1016/j.matlet.2016.07.004).
23. Aitola, K., Domanski, K., Correa-Baena, J.P., Sveinbjörnsson, K., Saliba, M., Abate, A., Grätzel, M., Kauppinen, E., Johansson, M.J., Tress, W., Boschloo, G. and Hagfeldt, A., "High temperature-stable perovskite solar cell based on low-cost carbon nanotube hole contact", ***Advanced Materials***, Vol. 29, No. 17, (2017), 1606398. (https://doi.org/10.1002/adma.201606398).
24. Meng, F., Gao, L., Yan, Y., Cao, J., Wang, N., Wang, T. and Ma, T., "Ultra-low-cost coal-based carbon electrodes with seamless interfacial contact for effective sandwich-structured perovskite solar cells", ***Carbon***, Vol. 145, (2019), 290-296. (https://doi.org/10.1016/j.carbon.2019.01.047).
25. Fagiolari, L. and Bella, F., "Carbon-based materials for stable, cheaper and large-scale processable perovskite solar cells, ***Energy & Environmental Science***, Vol. 12, No. 12, (2019), 3437-3472. (https://doi.org/10.1039/C9EE02115A).
26. Yang, Y., Xiao, J., Wei, H., Zhu, L., Li, D., Luo, Y., Wu, H. and Meng, Q., "An all-carbon counter electrode for highly efficient hole-conductor-free organo-metal perovskite solar cells", ***RSC Advances***, Vol. 4, No. 95, (2014), 52825-52830. (https://doi.org/10.1039/C4RA09519G).
27. Li, Z., Kulkarni, S.A., Boix, P.P., Shi, E., Cao, A., Fu, K., Wong, L.H., Xiong, Q., Zhang, J., Batabya, S.K., Mhaisalkar, S.G. and Mathews, N., "Laminated carbon nanotube networks for metal electrode-free efficient perovskite solar cells", ***ACS Nano***, Vol. 8, No. 7, (2014), 6797-6804. (https://doi.org/10.1021/nn501096h).
28. Wang, S., Jiang, P., Shen, W., Mei, A., Xiong, S., Jiang, X., Rong, Y., Tang, Y., Hu, Y. and Han, H., "A low-temperature carbon electrode with good perovskite compatibility and high flexibility in carbon based perovskite solar cells", ***Chemical Communications***, Vol. 55, No. 19, (2019), 2765-2768. (https://doi.org/10.1039/C8CC09905G).
29. Zhou, H., Shi, Y., Wang, K., Dong, Q., Bai, X., Xing, Y.,Du, Y. and Ma, T., "Low-temperature processed and carbon-based $ZnO/CH_3NH_3PbI_3/C$ planar heterojunction perovskite solar cells", ***The Journal of Physical Chemistry C***, Vol. 119, No. 9, (2015), 4600-4605. (https://doi.org/10.1021/jp512101d).
30. Kay, A. and Grätzel, M., "Low cost photovoltaic modules based on dye sensitized nanocrystalline titanium dioxide and carbon powder", ***Solar Energy Materials and Solar Cells***, Vol. 44, No. 1, (1996), 99-117. (https://doi.org/10.1016/0927-0248(96)00063-3).
31. Zhou, H., Shi, Y., Dong, Q., Zhang, H., Xing, Y., Wang, K., Du, Y. and Ma, T., "Hole-conductor-free, metal-electrode-free $TiO_2/CH_3NH_3PbI_3$ heterojunction solar cells based on a low-temperature carbon electrode", ***The Journal of Physical Chemistry Letters***, Vol. 5, No. 18, (2014), 3241-3246. (https://doi.org/10.1021/jz5017069).
32. Liu, Z., Shi, T., Tang, Z., Sun, B. and Liao, G., "Using a low-temperature carbon electrode for preparing hole-conductor-free perovskite heterojunction solar cells under high relative humidity", ***Nanoscale***, Vol. 8, No. 13, (2016), 7017-7023. (https://doi.org/10.1039/C5NR07091K).
33. Fu, H., "Review of lead-free halide perovskites as light-absorbers for photovoltaic applications: from materials to solar cells", ***Solar Energy Materials and Solar Cells***, Vol. 193, (2019), 107-132. (https://doi.org/10.1016/j.solmat.2018.12.038).
34. Etgar, L., Gao, P., Xue, Z., Peng, Q., Chandiran, A.K., Liu, B., Nazeeruddin, Md.K. and Grätzel, M., "Mesoscopic $CH_3NH_3PbI_3/TiO_2$ heterojunction solar cells", ***Journal of the American Chemical Society***, Vol. 134, No. 42, (2012), 17396-17399. (https://doi.org/10.1021/ja307789s).
35. Wang, H., Hu, X. and Chen, H., "The effect of carbon black in carbon counter electrode for $CH_3NH_3PbI_3/TiO_2$ heterojunction solar cells", ***RSC Advances***, Vol. 5, No. 38, (2015), 30192-30196. (https://doi.org/10.1039/C5RA02325D).
36. Ku, Z., Rong, Y., Xu, M., Liu, T. and Han, H., "Full printable processed mesoscopic $CH_3NH_3PbI_3/TiO_2$ heterojunction solar cells with carbon counter electrode", ***Scientific Reports***, Vol. 3, No. 3132, (2013). (https://doi.org/10.1038/srep03132).
37. Xu, M., Rong, Y., Ku, Z., Mei, A., Liu, T., Zhang, L., Li, X. and Han, H., "Highly ordered mesoporous carbon for mesoscopic $CH_3NH_3PbI_3/TiO_2$ heterojunction solar cell", ***Journal of Materials Chemistry A***, Vol. 2, No. 23, (2014), 8607-8611. (https://doi.org/10.1039/C4TA00379A).
38. Rong, Y., Ku, Z., Mei, A., Liu, T., Xu, M., Ko, S., Li, X. and Han, H., "Hole-conductor-free mesoscopic $TiO_2/CH_3NH_3PbI_3$ heterojunction solar cells based on anatase nanosheets and carbon counter electrodes", ***The Journal of Physical Chemistry Letters***, Vol. 5, No. 12, (2014), 2160-2164. (https://doi.org/10.1021/jz500833z).

39. Xu, M., Liu, G., Li, X., Wang, H., Rong, Y., Ku, Z., Hu, M., Yang, Y., Liu, L., Liu, T. and Chen, J., "Efficient monolithic solid-state dye-sensitized solar cell with a low-cost mesoscopic carbon based screen printable counter electrode", ***Organic Electronics***, Vol. 14, No. 2, (2013), 628-634. (https://doi.org/10.1016/j.orgel.2012.12.015).

40. Zhang, L., Liu, T., Liu, L., Hu, M., Yang, Y., Mei, A. and Han, H., "The effect of carbon counter electrodes on fully printable mesoscopic perovskite solar cells", ***Journal of Materials Chemistry A***, Vol. 3, No. 17, (2015), 9165-9170. (https://doi.org/10.1039/C4TA04647A).

41. Fu, Q., Tang, X., Huang, B., Hu, T., Tan, L., Chen, L. and Chen, Y., "Recent progress on the long-term stability of perovskite solar cells", ***Advanced Science***, Vol. 5, No. 5, (2018), 1700387. (https://doi.org/10.1002/advs.201700387).

42. Khenkin, M.V., Katz, E.A., Abate, A., Bardizza, G., Berry, J.J., Brabec, C. and Cheacharoen, R., "Consensus statement for stability assessment and reporting for perovskite photovoltaics based on ISOS procedures", ***Nature Energy***, Vol. 5, No. 1, (2020), 35-49. (https://doi.org/10.1038/s41560-019-0529-5).

43. Wang, Y., Wu, T., Barbaud, J., Kong, W., Cui, D., Chen, H., Yang, X. and Han, L., "Stabilizing heterostructures of soft perovskite semiconductors", ***Science***, Vol. 365, No. 6454, (2019), 687-691. (https://doi.org/10.1126/science.aax8018).

44. Wang, R., Mujahid, M., Duan, Y., Wang, Z.K., Xue, J. and Yang, Y., "A review of perovskites solar cell stability", ***Advanced Functional Materials***, Vol. 29, No. 47, (2019), 1808843. (https://doi.org/10.1002/adfm.201808843).

45. Hong, Q.M., Xu, R.P., Jin, T.Y., Tang, J.X. and Li, Y.Q., "Unraveling the light-induced degradation mechanism of $CH_3NH_3PbI_3$ perovskite films", ***Organic Electronics***, Vol. 67, (2019), 19-25. (https://doi.org/10.1002/solr.201900394).

46. Wu, X., Xie, L., Lin, K., Lu, J., Wang, K., Feng, W., Fan, B. and Wei, Z., "Efficient and stable carbon-based perovskite solar cells enabled by the inorganic interface of CuSCN and carbon nanotubes", ***Journal of Materials Chemistry A***, Vol. 7, No. 19, (2019), 12236-12243. (https://doi.org/10.1039/C9TA02014D).

47. Chu, Q.Q., Ding, B., Peng, J., Shen, H., Li, X., Liu, Y. and Catchpole, K.R., "Highly stable carbon-based perovskite solar cell with a record efficiency of over 18 % via hole transport engineering", ***Journal of Materials Science & Technology***, Vol. 35, No. 6, (2019), 987-993.(https://doi.org/10.1016/j.jmst.2018.12.025).

48. Wang, S., Liu, H., Bala, H., Zong, B., Huang, L., Guo, Z.A. and Zhang, Z., "A highly stable hole-conductor-free $Cs_xMA_{1-x}PbI_3$ perovskite solar cell based on carbon counter electrode", ***Electrochimica Acta***, Vol. 335, (2020), 135686. (https://doi.org/10.1016/j.electacta.2020.135686).

49. Chen, H. and Yang, S., "Stabilizing and scaling up carbon-based perovskite solar cells", ***Journal of Materials Research***, Vol. 32, No. 16, (2017), 3011-3020. (https://doi.org/10.1557/jmr.2017.294).

50. Yu, Z., Chen, B., Liu, P., Wang, C., Bu, C., Cheng, N. and Zhao, X., "Stable organic–inorganic perovskite solar cells without hole-conductor layer achieved via cell structure design and contact engineering", ***Advanced Functional Materials***, Vol. 26, No. 27, (2016), 4866-4873. (https://doi.org/10.1002/adfm.201504564).

51. Habisreutinger, S.N., Leijtens, T., Eperon, G.E., Stranks, S.D., Nicholas, R.J. and Snaith, H.J., "Carbon nanotube/polymer composites as a highly stable hole collection layer in perovskite solar cells", ***Nano Letters***, Vol. 14, No. 10, (2014), 5561-5568. (https://doi.org/10.1021/nl501982b).

52. Baranwal, A.K., Kanaya, S., Peiris, T.N., Mizuta, G., Nishina, T., Kanda, H. and Ito, S.,"100 °C thermal stability of printable perovskite solar cells using porous carbon counter electrodes", ***ChemSusChem***, Vol. 9, No. 18, (2016), 2604-2608. (https://doi.org/10.1002/cssc.201600933).

53. Wang, P., Chai, N., Wang, C., Hua, J., Huang, F., Peng, Y. and Cheng, Y.B., "Enhancing the thermal stability of the carbon-based perovskite solar cells by using a $Cs_xFA_{1-x}PbBr_xI_{3-x}$ light absorber", ***RSC Advances***, Vol. 9, No. 21, (2019), 11877-11881. (https://doi.org/10.1039/C9RA00043G).

54. Xiang, S., Li, W., Wei, Y., Liu, J., Liu, H., Zhu, L. and Chen, H., "Natrium doping pushes the efficiency of carbon-based $CsPbI_3$ perovskite solar cells to 10.7 %", ***iScience***, Vol. 15, (2019), 156-164. (https://doi.org/10.1016/j.isci.2019.04.025).

55. Liu, H., Bala, H., Zhang, B., Zong, B., Huang, L., Fu, W. and Zhan, Z., "Thickness-dependent photovoltaic performance of TiO_2 blocking layer for perovskite solar cells", ***Journal of Alloys and Compounds***, Vol. 736, (2018), 87-92. (https://doi.org/10.1016/j.jallcom.2017.11.081).

56. Gouda, L., Rietwyk, K.J., Hu, J., Kama, A., Ginsburg, A., Priel, M. and Zaban, A., "High-resolution study of TiO_2 contact layer thickness on the performance of over 800 perovskite solar cells", ***ACS Energy Letters***, Vol. 2, No. 10, (2017), 2356-2361. (https://doi.org/10.1021/acsenergylett.7b00718).

57. Sung, Y.M., "Deposition of TiO_2 blocking layers of photovoltaic cell using RF magnetron sputtering technology", ***Energy Procedia***, Vol. 34, (2013), 582-588. (https://doi.org/10.1016/j.egypro.2013.06.788).

58. Lee, M.M., Teuscher, J., Miyasaka, T., Murakami, T.N. and Snaith, H.J., "Efficient hybrid solar cells based on meso-superstructured organometal halide perovskites", ***Science***, Vol. 338, No. 6107, (2012), 643-647. (https://doi.org/10.1126/science.1228604).

59. Aharon, S., Gamliel, S., El Cohen, B. and Etgar, L., "Depletion region effect of highly efficient hole conductor free $CH_3NH_3PbI_3$ perovskite solar cells", ***Physical Chemistry Chemical Physics***, Vol. 16, No. 22, (2014), 10512-10518. (https://doi.org/10.1039/C4CP00460D).

60. Laban, W.A. and Etgar, L., "Depleted hole conductor-free lead halide iodide heterojunction solar cells", ***Energy & Environmental Science***, Vol. 6, No. 11, (2013), 3249-3253. (https://doi.org/10.1039/C3EE42282H).

61. Yue, G., Chen, D., Wang, P., Zhang, J., Hu, Z. and Zhu, Y., "Low-temperature prepared carbon electrodes for hole-conductor-free mesoscopic perovskite solar cells", ***Electrochimica Acta***, Vol. 218, (2016), 84-90. (https://doi.org/10.1016/j.electacta.2016.09.112).

62. Liu, Z., Sun, B., Shi, T., Tang, Z. and Liao, G., "Enhanced photovoltaic performance and stability of carbon counter electrode based perovskite solar cells encapsulated by PDMS", ***Journal of Materials Chemistry A***, Vol. 4, No. 27, (2016), 10700-10709. (https://doi.org/10.1039/C6TA02851A).

63. Chang, X., Li, W., Zhu, L., Liu, H., Geng, H., Xiang, S. and Chen, H., "Carbon-based $CsPbBr_3$ perovskite solar cells: All-ambient processes and high thermal stability", ***ACS Applied Materials & Interfaces***, Vol. 8, No. 49, (2016), 33649-33655. (https://doi.org/10.1021/acsami.6b11393).

64. Li, J., Yao, J.X., Liao, X.Y., Yu, R.L., Xia, H.R., Sun, W.T. and Peng, L.M., "A contact study in hole conductor free perovskite solar cells with low temperature processed carbon electrodes", ***RSC Advances***, Vol. 7, No. 34, (2017), 20732-20737. (https://doi.org/10.1039/C7RA00066A).

65. Meng, F., Liu, A., Gao, L., Cao, J., Yan, Y., Wang, N. and Ma, T., "Current progress in interfacial engineering of carbon-based perovskite solar cells", ***Journal of Materials Chemistry A***, Vol. 7, No. 15, (2019), 8690-8699. (https://doi.org/10.1039/C9TA01364D).

66. Xiao, Y., Wang, C., Kondamareddy, K.K., Liu, P., Qi, F., Zhang, H. and Zhao, X.Z., "Enhancing the performance of hole-conductor free carbon-based perovskite solar cells through rutile-phase passivation of anatase TiO_2 scaffold", ***Journal of Power Sources***, Vol. 422, (2019), 138-144. (https://doi.org/10.1016/j.jpowsour.2019.03.039).

67. Liu, J., Zhou, Q., Thein, N.K., Tian, L., Jia, D., Johansson, E.M. and Zhang, X., "In situ growth of perovskite stacking layers for high-efficiency carbon-based hole conductor free perovskite solar cells", ***Journal of Materials Chemistry A***, Vol. 7, No. 22, (2019), 13777-13786. (https://doi.org/10.1039/C9TA02772F).

68. Zong, B., Fu, W., Guo, Z.A., Wang, S., Huang, L., Zhang, B. and Zhang, Z., "Highly stable hole-conductor-free perovskite solar cells based upon ammonium chloride and a carbon electrode", ***Journal of Colloid and Interface Science***, Vol. 540, (2019), 315-321. (https://doi.org/10.1016/j.jcis.2019.01.035).

69. Zhang, X., Zhou, Y., Li, Y., Sun, J., Lu, X., Gao, X. and Liu, J.M., "Efficient and carbon-based hole transport layer-free $CsPbI_2Br$ planar perovskite solar cells using PMMA modification", ***Journal of Materials Chemistry C***, Vol. 7, No. 13, (2019), 3852-3861. (https://doi.org/10.1039/C9TC00374F).

70. Li, W., Huang, Y., Liu, Y., Tekell, M.C. and Fan, D.E., "Three dimensional nanosuperstructures made of two-dimensional materials by design: Synthesis, properties, and applications", ***Nano Today***, Vol. 29, (2019), 100799. (https://doi.org/10.1016/j.nantod.2019.100799).

71. Hammouda, S.B., Salazar, C., Zhao, F., Ramasamy, D.L., Laklova, E., Iftekhar, S. and Sillanpää, M., "Efficient heterogeneous electro-Fenton incineration of a contaminant of emergent concern-cotinine-in aqueous medium using the magnetic double perovskite oxide Sr_2FeCuO_6 as a highly stable catalayst: Degradation kinetics and oxidation products", ***Applied Catalysis B: Environmental***, Vol. 240, (2019), 201-214. (https://doi.org/10.1016/j.apcatb.2018.09.002).

72. Hu, Y., Schlipf, J., Wussler, M., Petrus, M.L., Jaegermann, W., Bein, T. and Docampo, P., "Hybrid perovskite/perovskite heterojunction solar cells", ***ACS Nano***, Vol. 10, No. 6, (2016), 5999-6007. (https://doi.org/10.1021/acsnano.6b01535).

73. Yu, H., Liu, X., Xia, Y., Dong, Q., Zhang, K., Wang, Z. and Li, Y., "Room-temperature mixed-solvent-vapor annealing for high performance perovskite solar cells", ***Journal of Materials Chemistry A***, Vol. 4, No. 1, (2016), 321-326. (https://doi.org/10.1039/C5TA08565A).

74. Siddique, M.N., Ahmed, A. and Tripathi, P., "Electric transport and enhanced dielectric permittivity in pure and Al doped NiO nanostructures", ***Journal of Alloys and Compounds***, Vol. 735, (2018), 516-529. (https://doi.org/10.1016/j.jallcom.2017.11.114).

75. Beegum, K.B., Paulose, M., Peter, V.J., Raphael, R., Sreeja, V.G. and Anila, E.I., "Study on the effect of synthesis temperature on the structural and surface morphological and optical properties of methyl ammonium lead iodide nanoparticles by sol-gel method", ***IOP Conference Series: Materials Science and Engineering***, Vol. 149, ***International Conference on Advances in Materials and Manufacturing Applications (IConAMMA-2016)***, Bangalore, India, (2016), p. 012078. (https://doi.org/10.1088/1757-899X/149/1/012078).